Jordan Journal of Civil Engineering, Volume **16**, No. **3**, **2022**

Effect of NSM Technique on Moment Redistribution in Top Strengthened RC Continuous Beams

Shady Salem [1], ***Amr Ibrahim*** [1)*], ***Mahmoud El-Kateb*** [2], ***Ayman Khalil*** [2] ***and Mohamed Attia*** [3]

[1)] The British University in Egypt, Department of Civil Engineering, Cairo, Egypt.
* Corresponding Author: amr.ibrahim@bue.edu.eg
[2)] Department of Civil Engineering, Ain Shams University, Cairo, Egypt.
[3)] Department of Civil Engineering, Canadian International College, Cairo, Egypt.

ABSTRACT

Abundant research has been presented addressing the strengthening of continuous reinforced concrete (RC) beams depending on the moment-redistribution (MR) effect. Most of the research was backed on either strengthening the bottom surface of the beam or both the top and bottom surfaces. As such, both techniques require full accessibility for the beam bottom surface, which may not be applicable. This paper presents a novel strengthening technique using near-surface mounted steel or fiber-reinforced polymer (FRP) laminates. The present study assesses experimentally/numerically the behavior of RC continuous beams top-strengthened at the hogging regions only. The experimental process includes testing five full-scale RC continuous beams strengthened with either steel plates or carbon-fiber-reinforced polymer (CFRP) laminates. Moreover, the numerical model is developed using a finite element (FE) program and used for parametric investigation to assess the strengthening efficiency under different parameters. Strengthening using glass fiber-reinforced polymer (GFRP) laminates was also investigated in the numerical analysis. Strengthening using steel plates caused up to fifty percent moment redistribution with a significant increase in the load-carrying capacity of the beams. On the other hand, CFRP- and GFRP-strengthened beams showed substantial amounts of moment redistribution without significantly affecting the load-carrying capacity.

KEYWORDS: Moment redistribution, Strengthening, Near-surface mounting, Numerical analysis, Steel plates, FRP laminates.

INTRODUCTION

Over the decades, strengthening of concrete structures has been extensively studied by proposing new strengthening techniques or assessing parameters influencing the efficiency of different strengthening techniques. Several researchers accounted for moment redistribution (MR) that may occur in indeterminant concrete structures as a strengthening approach through different techniques. For example, the efficiency of strengthening reinforced concrete (RC) beams was investigated using externally bonded steel plates to allow MR to occur (Aykac et al., 2013; Rakgate and Dundu, 2018). Farahbod and Mostofinejead (2011) experimentally assessed MR for six two-span frames strengthened with fiber-reinforced polymers (FRP). Lou et al. (2014) and Liu (2006) addressed MR for RC continuous beams and slabs due to application of FRP/steel on their surface, whereas Kara and Ashour (2013) numerically assessed MR of continuous beams reinforced with FRP. Akiel et al. (2018) examined MR of hybrid RC continuous beams reinforced with basalt fiber-reinforced polymer and conventional reinforcement, while Rahman et al. (2017) assessed MR for FRP-reinforced concrete beams under unsymmetrical loadings. Moreover, Li et al. (2019) introduced a state-of-the-art review for the experimental/numerical testing of RC continuous members, e.g. beams and slabs. However, most of the published work accounts for strengthening either both hogging and sagging sides or sagging sides only. As

Received on 7/1/2022.
Accepted for Publication on 29/4/2022.

such, the previously reported strengthening techniques would require full accessibility for the sagging sides; i.e., the bottom side of the concrete element, which may not be applicable in certain structures.

Scholz (1993) and Camaro and Lopes (2008) reported that MR happened for different concrete elements after surpassing the elastic stage due to the difference in stiffness between the hogging and sagging sections. Typically, MR occurs by transferring the moment demand from the hogging side to the sagging side in order to reach equilibrium. However, in some cases, increasing the hogging moment rather than the sagging moment is required instead. Subsequently, this MR criterion facilitates the strengthening of the hogging zones, which may only be needed for strengthening concrete elements with inaccessibility from the lower side.

On the other hand, various researchers have investigated the application of different strengthening techniques to assess MR for indeterminant structures. Oehlers et al. (2004a, b) observed significant MR by strengthening RC members with conventional steel plates, which showed sufficient bond strength that allowed full utilization of MR in the tested members. Alternatively, beams strengthened with carbon-fiber-reinforced polymer (CFRP) using externally bonded plates showed debonding at relatively low strains (Ibrahim et al., 2020; Liu et al., 2006; Ashour et al., 2004; El-Refaie et al., 2003). However, near-surface mounted (NSM) CFRP plates showed debonding at high strains resulting in significant amounts of MR (Ibrahim et al., 2020; Ibrahim et al., 2020; De Lorenzis et al., 2002; Hassan and Rizkalla, 2003). Ibrahim et al. (2020) experimentally tested eight beams strengthened with either steel or CFRP plates bonded on the top surface or through the NSM plating technique at the hogging zone only. The results showed a good effect of the application of NSM laminates on the resulting MR. However, these results were presented in comparison to that of the control specimen, which may not be a good representation for assessing the strengthening techniques. Moreover, a parametric numerical investigation was presented for steel and CFRP plates bonded on the top surface or through NSM continuous beams (Ibrahim et al., 2020). This paper investigates the effect of top NSM strengthening on MR in RC continuous beams. Strengthening is applied at the hogging zones only and will be *via* the application of either steel plates, CFRP or GFRP laminates.

EXPERIMENTAL PROGRAM

1) Test Specimens

Five two-span continuous beams with 2000 mm span were tested under monotonic quasi-static loading and were loaded at the center of each span. Figure 1 depicts the test specimens' configuration, support locations, reinforcement details and strengthening location (at the hogging zones only).

All beams were designed using the effect of an adjacent slab (T-sections) to avoid early flexural failure at the mid-span segment, allowing for greater quantities of MR. As indicated in Figure 2, the width of the beams was 200 mm and the thickness was 350 mm. The width of flanges was 400 mm and they were 8 mm in thickness, while the concrete cover from all sides of the beam web and flanges was 15 mm. The plates used for strengthening were connected to the beam flanges within the effective width of the beam to simulate the avoidance of the presence of an intermediate column. The flexural reinforcement at the upper and bottom sides of the beams consisted of four rebars, each 10 mm in diameter, throughout the entire length of the specimens. The top side of the steel plate beam used in strengthening was 1500 mm in length at the position of the intermediate support to cover the entirety of the testing beams' hogging zones. The transverse shear reinforcement consisted of stirrups with a diameter of 8 mm spaced at 100 mm to avoid any premature shear failure during beam testing. Additional reinforcement of eight rebars, each 8 mm in diameter, was distributed inside the flanges, with four rebars on each side, as shown in the cross-section in Figure 2. The transverse reinforcement in the concrete flanges was composed of mild steel bars 8 mm in diameter, spaced at 100 mm.

Table 1 shows the test matrix and illustrates the experimental parameters of the five beams. Beam B1 was the control specimen without any form of strengthening. The other specimens were reinforced with one or two NSM steel plates or CFRP laminates. The labeling system for strengthened beams is determined by the type and number of strengthening plates used. These symbols begin with the letter C (carbon) or S (steel) based on the plate's material and are

followed by a numeral denoting the number of used plates; e.g. beam C1 is reinforced with one NSM CFRP plate and beam S2 is reinforced with two NSM steel plates. The dimensions of the steel plate were 50 mm in width and 6 mm in thickness, whereas the dimensions of the CFRP plate were 50 mm in width and 1.2 mm in thickness. To enhance the connection with the concrete surface, both carbon and steel plates were covered with an epoxy adhesive material.

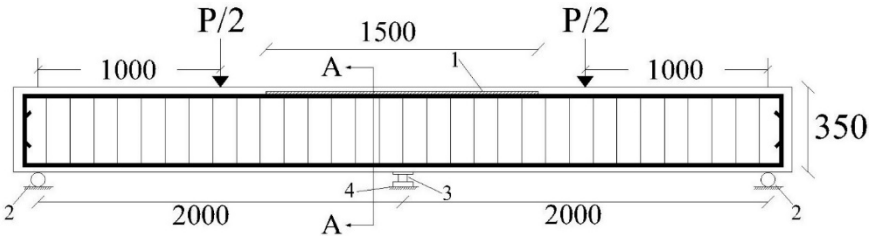

Figure (1): Test setup (all dimensions in mm). 1 - Steel plate / FRP laminate; 2 - roller support, 3 - load cell, 4 – hinged support

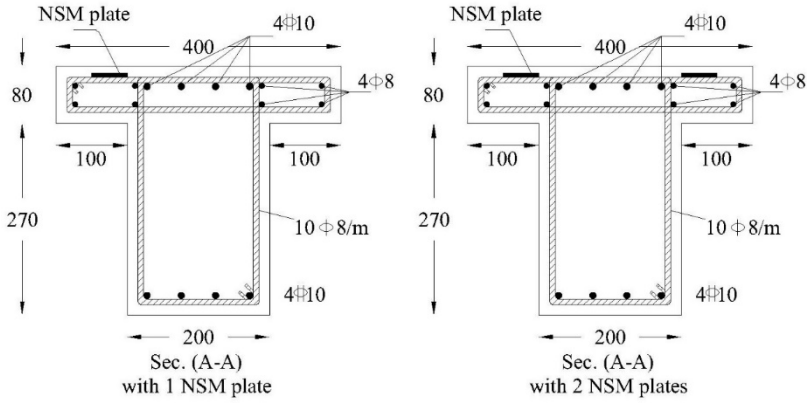

Figure (2): Cross-sections (dimensions in mm)

Table 1. Test matrix

Specimen	Material of plates	Number of plates
B1	N/A (Control)	---
S1	Steel	1
S2	Steel	2
C1	CFRP	1
C2	CFRP	2

2) Instrumentation and Loading Protocol

The loading scheme of the tested beams is further illustrated in Figure 3. Two load cells were used: one at the loading jack to measure the whole load applied and the other at the intermediate support to measure the vertical response of the central support. The specimens were tested under four-point loading in a static monolithic way until failure. A total of six (LVDTs) with 0.01-mm accuracy were used to measure the vertical displacements at fixed points along the beam length. Two LVDTs were used under the points of load application and the four remaining LVDTs were installed at equal distances of 500 mm. Three electrical concrete strain gauges (CS) were bonded to the concrete surface. Two gauges were fixed on the top surface of the concrete at the sagging zones, while the third one was fixed at the bottom layer of the beams near the central support. Six electrical steel stain gauges were applied on the main upper and main lower longitudinal reinforcement as well as on the strengthening plates using a quick setting epoxy. Four of them were installed to the lower steel reinforcement; one gauge was applied to the upper reinforcement at the central support section, while the final gauge measured the tensile strain of the implemented plates in the strengthened beams.

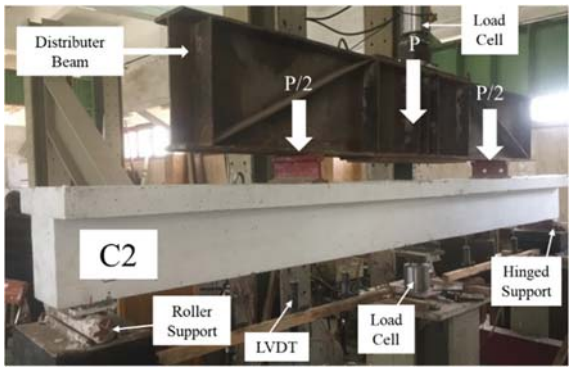

Figure (3): Test setup

Material Properties

The used concrete had a characteristic compressive strength of 28.72 MPa, according to the British Standards (BS, 2009), while the average density of the concrete was 22.64 kN/m^3. The high-strength steel rebars, used as the longitudinal reinforcement, had 360 MPa yield stress and 520 MPa ultimate tensile strength, while yield and ultimate strengths of mild steel, used as transverse reinforcement in the web and flanges, were 240 and 350 MPa, respectively. As for the strengthening steel plates, coupon specimens (ASTM, 2000) were tested and resulted in yield and ultimate strength of 425 and 566 MPa, respectively. According to the manufacturer's data, the ultimate tensile strength of the CFRP laminates was 3100 MPa and the modulus of elasticity was 165 GPa.

Experimental Observations

1) Failure Modes

All strengthened specimens had the same crack pattern and flexural behavior, with cracks beginning at the section of load application and extending to the support section. Cracks were observed at the load application points at load levels of about 160 kN, followed by the central support at load values of about 300 kN. As illustrated in Figure 4, the collapse in the control beam began with concrete crushing in the positive moment zones at 435 kN. Regarding crack initiation, pattern and failure mode, the reinforced beams S1, C1 and C2 behaved similarly to the control specimen, as shown in Figure 5. However, as seen in Figure 6, beam S2 failed at the middle support section by crushing the concrete at the beam's lower soffit.

Figure (4): Beam B1 at failure

Figure (5): Typical failure pattern for beams S1, C1 and C2

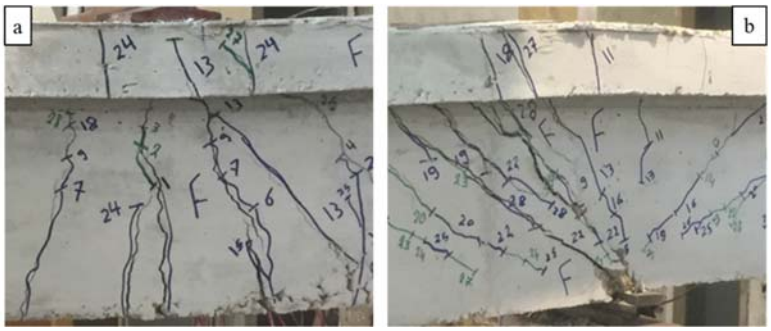

Figure (6): Failure mode of S2 a) at the middle of the span; b) at the intermediate support

2) Test Results

The experimental findings are summarized in Table 2, with P_u representing the highest load applied to the beam and R_m representing the vertical response of the intermediate support at load P_u. M_{sag} and M_{hog} are the experimental flexural moments at the mid-span and central support locations, respectively. $M_{sag.el}$ and $M_{hog.el}$ are the flexural bending moments in the sagging and hogging regions, computed using Equations (1) and (2), which were established by Aiello et al. and are based on linear elastic analysis. The symbol *l* represents the clear span length, while *a* is the distance from the applied load to the edge support. It is worth noting that Equations 1 and 2 ignore the impact of the own weight and assume constant stiffness throughout the length of the beam, while [%] of change, M_{sag} and [%] of change, M_{hog} indicate the percentage of moment change in the sagging and hogging zones with respect to the elastic state and are computed using Equations (3) and (4).

$$M_{sag.el} = \frac{(2l^3 - 3al^2 + a^3)}{4l^3} aP_u \quad (1)$$

$$M_{hog.el} = -\frac{a(l^2 - a^2)}{4l^2} P_u \quad (2)$$

$$[\%]\ of\ change, M_{sag} = \left(\frac{M_{sag} - M_{sag.el}}{M_{sag.el}}\right) * 100 \quad (3)$$

$$[\%]\ of\ change,\ \ M_{hog} = \left(\frac{M_{hog} - M_{hog.el}}{M_{hog.el}}\right) * 100 \quad (4)$$

From Table 2, beams strengthened with steel plates had more ultimate load values and MR percentages compared to beams strengthened with CFRP plates despite having the same number of plates. The failure load and the average percentage of MR in beam SN1 were 4% and 13%, respectively and were higher than those of C1, whereas the ultimate load and average percentage of MR in S2 were higher than those of C2 by 20% and 33%, respectively. Furthermore, it may be concluded that using two plates/laminates is more effective than using just one (whether steel or carbon). This was supported by the fact that beam S2 had greater percentages of load capacity increase, M_{sag} decrease and M_{hog} increase than beam S1 by 17%, 8% and 31%, respectively. Furthermore, beam C2 had greater MR percentages than C1 with an 11% higher increase in the average percentage of MR. However, the use of NSM CFRP laminate had no effect on the load-carrying capabilities of the beams, as the ultimate loads in beams C2 and C1 were similar to that in the control beam B1.

Table 2. Test results

Specimen	P_u	$M_{sag.}$	$M_{hog.}$	$M_{sag.el}$	$M_{hog.el}$	[%]change, M_{sag}	[%]change, M_{hog}	Average [%] of MR
	kN	kN.m						
B1	467	53.40	-126.81	73.00	-87.60	-27	45	36
S1	481	44.67	-151.10	75.13	-90.16	-41	68	54
S2	561	41.21	-198.27	87.71	-105.26	-53	88	71
C1	462	46.22	-138.71	72.23	-86.68	-36	60	48
C2	469	44.07	-146.14	73.21	-87.85	-40	66	53

Analysis of Experimental Results

1) Strains

Figure 7 illustrates the applied loads measured against the tensile strain of the lower reinforcement at the sagging zones, while Figure 8 shows the applied loads measured against the compressive strain of concrete bottom side at the central support. Since ductility is a key factor for MR to occur and all beams were pre-designed to have enough ductility to allow for MR to take place, the figure exhibits a consistent pattern for all beams, with the exception of S2, which had a slight yielding plateau. This distinct behavior supports the notion that the ductility of this beam was limited by the concrete crushing at the central support. It was also observed that the use of CFRP plates had no effect on the load-strain relationship in the linear elastic stage, as illustrated in beams C1 and C2.

2) Deflections

Figure 9 illustrates the load-deflection graphs for the tested beams at the load application locations. The control specimen B1 had the greatest vertical displacement of

27.15 mm. It is worth noting that the use of both steel and CFRP strengthening had no effect on the flexural stiffness of the beams during the linear elastic stage, as all of the beams initially behaved elastically until reaching a value between 300 and 360 kN. When compared to the control specimen, all of the reinforced beams exhibited lower values of ultimate displacement. This is mostly due to moment transfer from sagging to hogging zones and indicates that reducing sagging moments resulted in lower deflection values at the sagging portion of the load application location.

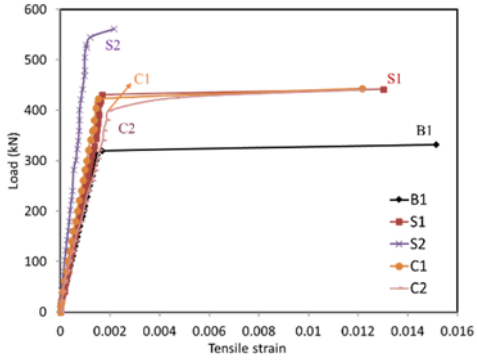

Figure (7): Applied load *vs.* tensile strains of bottom reinforcement

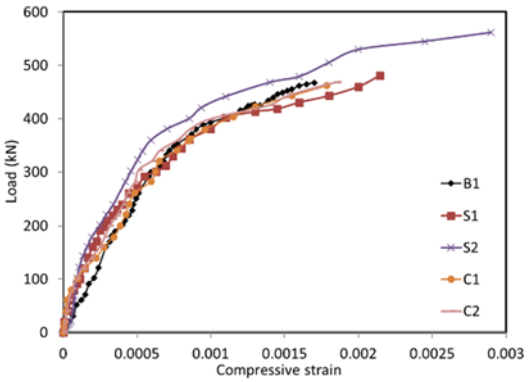

Figure (8): Applied load *vs.* compressive strain of concrete bottom side at the central support

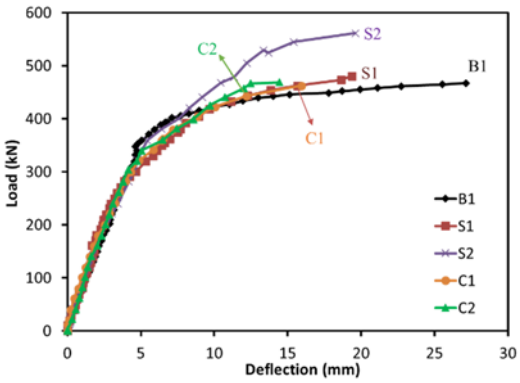

Figure (9): Load-deflection curves for the tested beams

3) Load *vs.* Percentage of MR

Figure 10 illustrates the relationship between the applied load and the average percentage of MR, compared to the elastic state, for the tested beams. The control beam started with negative values of average MR, meaning that the average values of the experimental flexural moments were less than those of the elastic ones until reaching 120 kN. Subsequently, the MR begins to exist within the positive range indicating MR from the sagging zone to the hogging zone. MR tends to be constant between 210 and 320 kN, which is backed to the yielding plateau of the positive lower reinforcement. Finally, the MR percentages continue to increase until the end of the loading. Similarly, beam S1 behaved in the same manner as beam B1, except that the values of average MR continued to rise after they turned to the positive side until failure took place. The average percentages of MR for beam S2 increased steadily with load increase during the test. The values of average MR for beams C1 and C2 were decreasing at the beginning of the test until reaching load levels of about 320 and 340 kN for C1 and C2, respectively, at which the lower steel reinforcement began to yield. As a result, the values started to increase until reaching the failure load.

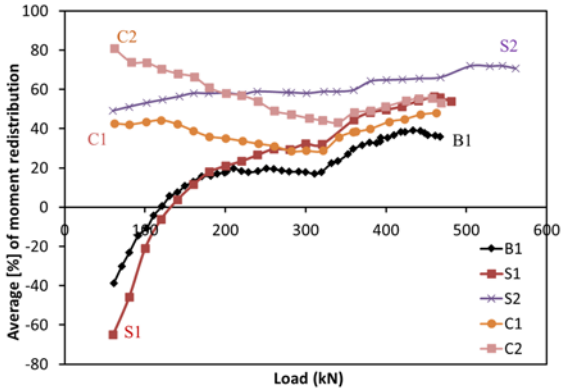

Figure (10): Applied loads *vs.* average % of MR

Numerical Modeling (Finite Element Modeling)

The five tested beams were modeled using the finite element program ABAQUS 6.14 (ABAQUS, 2014) to analyze RC continuous beams top-retrofitted with NSM plates/laminates. In terms of load-deflection and load-strain relationships, the FE model findings were validated against the experimental data. The accuracy of the findings is mostly influenced by the FE mesh size, constitutive models for material and boundary conditions (Lasheen et al., 2018; Ismail et al., 2020;

Fouda et al., 2021). As a result, the suggested FE model fully examined these issues and sensitivity analysis was conducted for the modeling parameters. A well-known hexahedral mesh with a 50 mm size is chosen. The strengthening plates were described as solid homogenous parts, whereas linearly ordered three-dimensional trussed elements were used to represent the reinforcement bars and shear stirrups.

1) Steel Modeling

The longitudinal reinforcement rebars and shear stirrups were modeled as truss wires, whereas the additional steel plates were represented as solid homogenous parts. Both the steel reinforcement and steel plates were defined as perfect elasto-plastic materials. The relation between stress and strain was assumed to be bilinear in tension. The modulus of elasticity and Poisson's ratio for both materials were 200 GPa and 0.2, respectively. The yield strength for the steel rebars was 360 MPa, while the yielding strength for the steel plates was 425 MPa. For the mild steel used in the transverse shear stirrups and the reinforcement of the beam flanges, the yield strength was 240 MPa and it had the same modulus of elasticity and Poisson's ratio as the steel reinforcement bars and steel plates.

2) Concrete Modeling

A concrete-damaged plasticity was implemented in the developed model. The dilation angle was considered 38°, while the eccentricity and f_{b0}/f_{c0}; i.e., the ratio of the biaxial strength to the uniaxial strength, were taken as 1 and 1.12, respectively. Moreover, the distance ratio of the hydrostatic axis and the deviatoric cross-section (K) was taken as 0.67 and the viscosity parameter was considered 0.01. Modeling of the compressive behavior of concrete was carried out according to Wight and James (2012) and the tensile behavior of concrete was modeled based on the concrete tensile stress (σ_t), which decreases gradually as cracks occur. Tension stiffening was also considered to represent the concrete tensile behavior across cracks after failure. The uniaxial variables for compression damage (d_c) and tension damage (d_t) were calculated using the mathematical equations developed by Jankowiak et al. (2005).

3) CFRP Laminates Modeling

The CFRP laminates were defined as solid homogeneous parts and C3D8R elements with size 50 mm were used in meshing the laminates. The modeled CFRP material possessed no yielding characteristics and the elastic properties were 165 GPa for Young's modulus and 0.2 for Poisson's ratio. The ultimate strength of the CFRP material was 3100 MPa.

4) Interaction between Concrete and Steel Reinforcement

The steel reinforcements were modeled as embedded elements inside the concrete beam using the embedded element constraint. The concrete-steel reinforcement interaction was defined using a truss in solid elements. The reinforcement steel bars were stimulated by truss wires as embedded regions, while the concrete beam, or host element, was defined as a continuous solid homogeneous element.

5) Contact between Concrete and Strengthening Plates/Laminates

The contact between concrete and the strengthening elements was simulated by both tangential and cohesive behaviors to reflect the debonding of the plates/laminates from the concrete. For the cohesive contact, the damage initiation was taken as 6 MPa under shear stresses and 4 MPa under normal stresses. The coefficient of viscosity in damage stabilization was 1E-5, while the ratio between the total and plastic displacements was 0.1. The tangential behavior had a coefficient of penalty friction of 0.5.

6) Loading and Boundary Conditions

A displacement control loading was applied in the vertical axis on two cutting planes at the midpoint of each span. For all the developed models, a two-hundred loading increment was applied using a dynamic/explicit loading with a step time of 4 seconds. The linear and quadratic bulk viscosity parameters were 0.06 and 1.2, respectively. The non-linearity for the materials was taken into consideration to account for the second-order effects. Smooth-step amplitude was also used to define the displacement loading of the beams. The failure loads were determined from the vertical reaction forces in the Y-direction (RF2) at the reference points that were established for the displacement loading. As for the supports, displacement/rotation boundaries were applied to mimic the experimental boundary conditions.

Model Validation

The results of the developed finite element models were compared with the experimental test results in terms of the load-carrying capacities, mid-span deflections, elastic stiffnesses and failure modes. The following section summarizes the comparison between the results of the developed FE models and the conducted experimental work. Furthermore, the developed models were used to introduce a comprehensive parametric investigation for the proposed strengthening techniques.

1) Strength of Beams

Table 3 summarizes the failure load for each beam in both the experimental program and the finite element analysis (FEA). The loads shown in the table are for the failure loads at each span (0.5 P_u). The failure loads obtained from the FEA represent the load values at which the FE model could not reach convergence; i.e., neither the concrete compressive nor the steel reinforcement tensile strains have reached their ultimate capacity. Table 4 shows the ratio of the FE results against the experimental results. It was found that the average difference between the FE and experimental results was 5.91 % with a 7.24 % standard deviation.

Table 3. FE *vs.* experimental results

Beam	Ultimate load capacity of each span $0.5P_u$ (kN)		Stiffness at elastic zone $(0.5P/\Delta)_{el.}$ (kN/mm)		Maximum vertical displacement (Δ_u) (mm)		% (Num./Exp.)		
	Num.	Exp.	Num.	Exp.	Num.	Exp.	$0.5P_u$	$(0.5P / \Delta)_{el.}$	Δ_u
B1	225	234	40.63	35.87	29.78	27.15	96	113.	110
S1	285	240	34.47	32.12	19.98	19.36	119	107	103
S2	299	281	36.9	32.98	22.02	19.61	107	112	112
C1	238	231	36.43	34.68	15.99	15.93	103	105	100
C2	246	234	41.29	36.75	16.02	14.44	105	112	111
					Average		106	110	107
					Standard deviation		7	3	5

2) Deflection and Elastic Stiffness

Table 3 shows the maximum vertical displacement values for all beams and the ratio of numerical to experimental findings. It also summarizes the elastic stiffness computed for the developed models and compared to the experimental findings. According to the findings, the average results deviation for the ultimate vertical displacement is 10%, with a standard deviation of approximately 5%. For the final vertical displacement, the average variation between the numerical and experimental findings is 7%, while for the elastic stiffness values, the difference between both sets of results is 10 % with a standard deviation of 7%.

Figure 11 depicts the load-deflection behavior for both the experimental results and numerical models' findings. According to the load-deflection graphs, there is solid agreement between the experimental and numerical findings, particularly in the elastic stage. As such, the numerical load values in beams S1 and S2 start to slightly exceed the experimental load values. However, it was observed that the load-deflection behavior of beam B1 was similar during the elastic stage, followed by lower values for the numerical loads until failure. This behavior is attributed to the bi-linear behavior considered when modeling the steel reinforcement. It is worth mentioning that the FE models were able to estimate the failure loads at nearly the same experimental maximum deflection for all beams.

3) Failure Modes

All the developed FE models underwent the same failure sequence as in the experimental program, in which the failure commenced through yielding of reinforcement steel near the load application points. The FE yielding loads of the upper and lower steel reinforcement were recorded at almost the same level as the experimental results. Moreover, the experimental and FE final failure modes were also the same in all the

tested beams. The typical failure mode for beams B1, S1, C1 and C2 at which the tension damage governed final failure in both the experimental and FE results is shown in Figure 12. Figure 13 illustrates the compression damage for S2, governed by concrete crushing, both experimentally and numerically and demonstrates a validation for their failure modes. As such, the developed FE models' outcomes were in strong agreement with the experimental findings. Consequently, the developed FE models are implemented to extend the current study by evaluating the effect of different parameters on the resulting MR, as well as the flexural behavior of RC continuous top-strengthened beams.

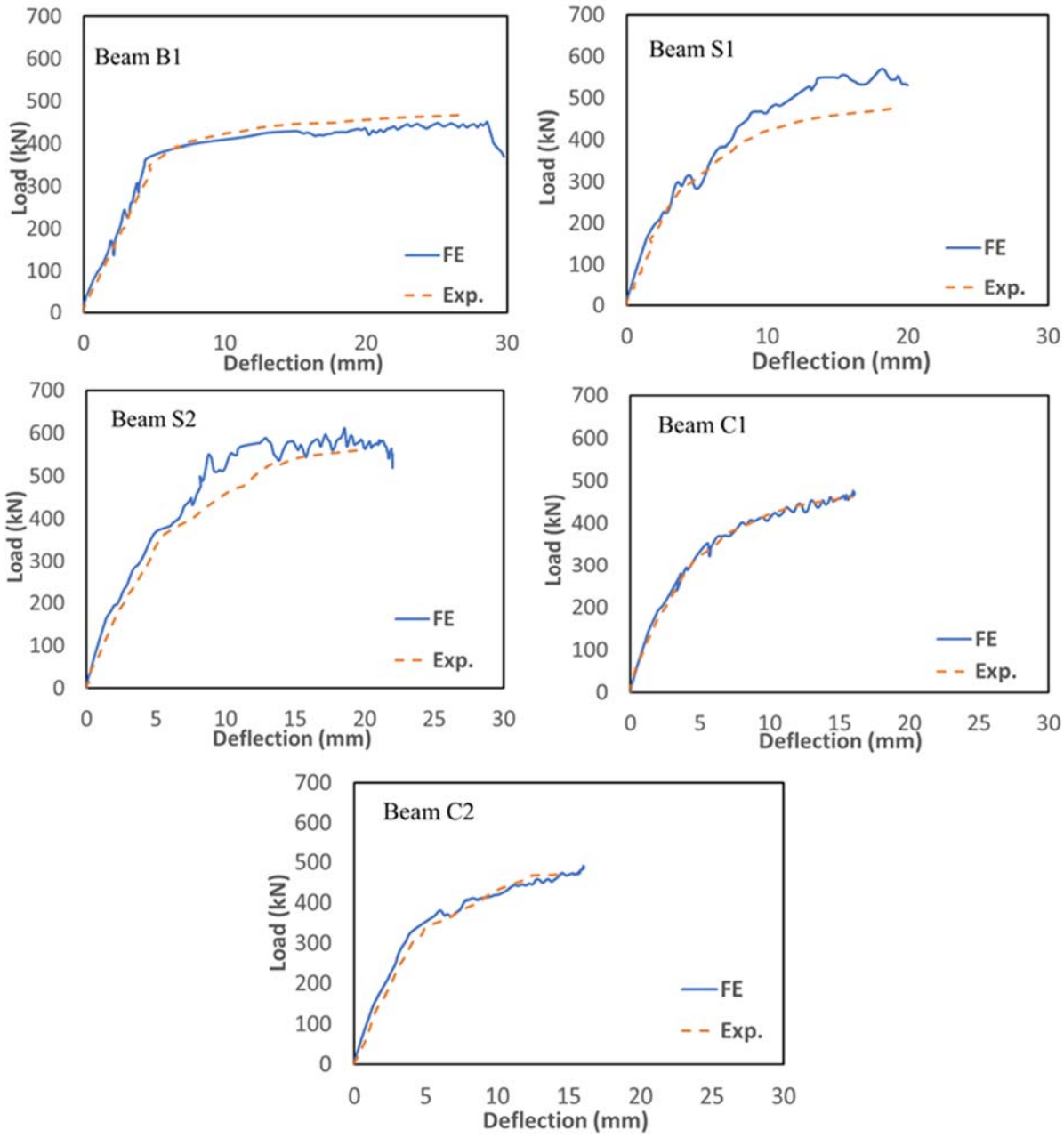

Figure (11): Applied loads vs. maximum deflection relationships (FE vs. Exp.)

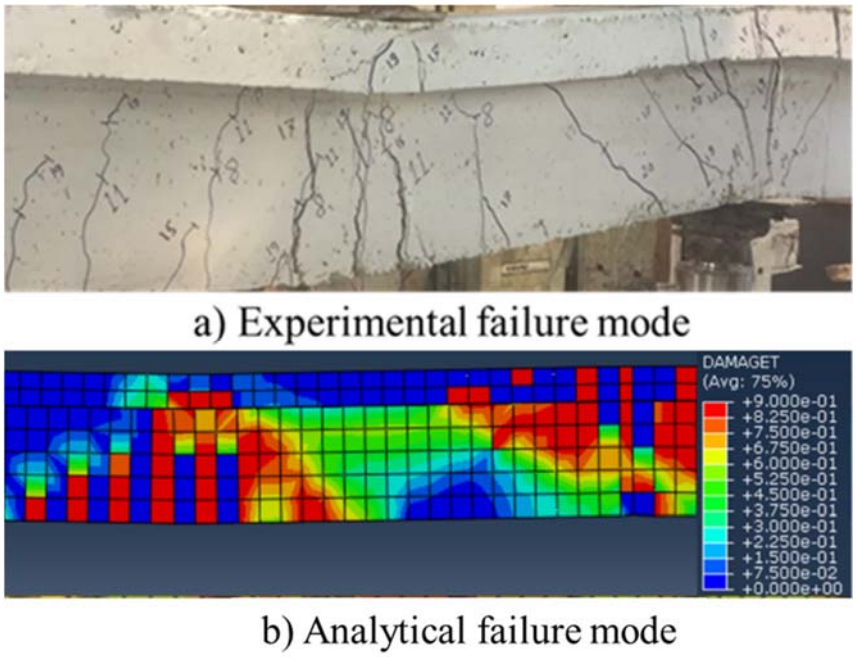

Figure (12): Typical failure pattern for beams B1, S1, C1 and C2

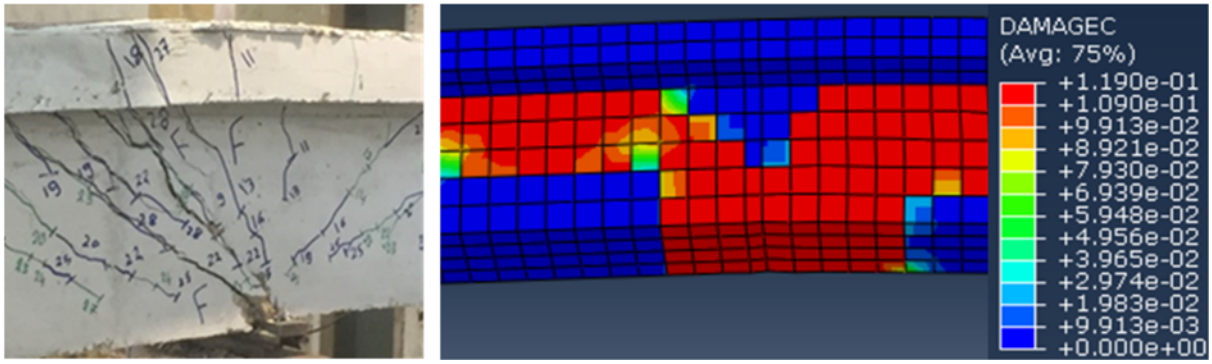

Figure (13): Concrete failure (compression damage) in beam S2

Parametric Study Analysis

On 27 continuous beams, a parametric analysis was conducted to evaluate the effect of different factors on MR in strengthened beams with the NSM top-plated technique. As indicated in Table 4, the parameters assessed were concrete compressive strength (f_{cu}), reinforcement ratio (μ), beam thickness (t_b) and thickness of strengthening plates/laminates (t_{pl}). Two NSM steel plates were applied to specimens B1' to B9, while specimens B10 to B18 were retrofitted by two NSM CFRP laminates and specimens B19 to B27 were strengthened using two NSM GFRP laminates. The GFRP laminates were defined in the FE models as solid homogeneous parts with no yielding characteristics. The elastic properties of the GFRP laminates were 42 GPa for Young's modulus and 0.2 for Poisson's ratio, while the ultimate strength was 945 MPa.

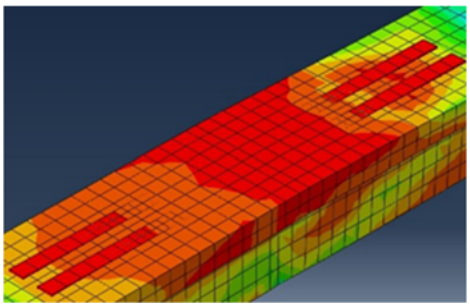

Figure (14): CFRP laminates debonding in B18

Parametric Study Results

The findings of the beams investigated in the parametric analysis, including the achieved bending moment redistribution for each beam, are provided in

this section. The vertical force reactions at the intermediate support and at the load application points are determined from the FE models and the bending moments for the beams were calculated using basic statistics. $M_{sag(FE)}$ and $M_{hog(FE)}$ represent the sagging and hogging bending moments obtained from the FE models. $M_{sag.el}$, $M_{hog.el}$ and the percentage of change in M_{sag} and M_{hog} were calculated using Equations 1- 4. The percentage enhancement in MR was determined relative to B1', B10 and B19 for specimens B2 to B8, B11 to B18 and B20 to B27, respectively. All percentages of MR achieved by beams B1' to B27 are shown in Figure 15. The beams strengthened with steel plates are compared with their counterpart beams strengthened with CFRP and GFRP laminates. For example, B2 is compared with B11 and B20 because the only difference between these three beams is the material of the strengthening plate, while they share the same parameters investigated in this parametric study, which are f_{cu}, μ, t_b and t_{pl}. The only exception is the thickness of the plates, as the thicknesses of steel plates investigated were 6, 8 and 10mm, while the thicknesses of the CFRP and GFRP laminates were 1.2, 1.8 and 2.6 mm. Therefore, the beams strengthened with 6mm, 8mm and 10 mm steel plates are compared with those strengthened with 1.2mm, 1.8mm and 2.6mm FRP laminates, respectively.

Table 4. Parametric study matrix

Specimen ID			Concrete compressive strength (f_{cu}) (MPa)	Upper & lower reinforcement (rft. Ratio (μ))	Thickness of beam (t_b) (mm)	Plate/laminate thickness (t_{pl})	
Specimens with steel plates	Specimens with CFRP laminates	Specimens with GFRP				Steel plates	CFRP / GFRP laminate
B1'	B10	B19	25	4T10 (0.47%)	350	6	1.2
B2	B11	B20	35				
B3	B12	B21	45				
B4	B13	B22	25	4T12 (0.67%)			
B5	B14	B23		4T16 (1.2%)			
B6	B15	B24		4T10 (0.47%)	450		
B7	B16	B25			550		
B8	B17	B26			350	8	1.8
B9	B18	B27				10	2.6

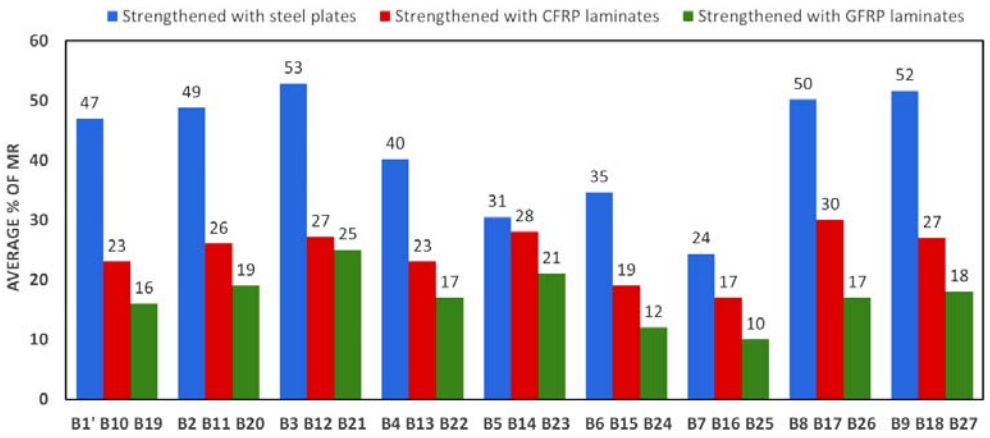

Figure (15): MR percentages for NSM-strengthened beams

1) Specimens with NSM Steel Plates

From Table 5, MR percentages were higher when increasing f_{cu} as observed from the findings of specimens B1', B2 and B3. The retrofitted beams with two steel plates in the experimental test program failed after concrete crushing at the lower side of load application section; thus, increasing f_{cu} will postpone concrete crushing at the intermediate support section. It was also observed that the reinforcement ratio is inversely proportional to MR, as depicted in the results of specimens B1, B4 and B5. This is

because increasing the reinforcement ratio increases the section tensile capacity at the tension side, subsequently increasing the corresponding compatibility compression forces in the concrete. The increase in the compression forces will result in early concrete crushing prior to the full utilization of MR. Furthermore, MR was reduced in the specimens with higher thicknesses, but was noticeably enhanced when increasing the strengthening plate thickness due to the increased variation in flexural stiffness between the strengthened and non-strengthened sections.

2) Specimens with NSM CFRP Laminates

Similarly, Table 6 summarizes the results of the CFRP-strengthened beams under the investigated parameters. It can be inferred that MR improved by increasing f_{cu} as shown in Beams B10, B11 and B12. In addition, increasing μ has enhanced the resulting MR, which opposes the behavior of beams strengthened with steel plates. This contradicting behavior is attributed to the fact that the beams retrofitted by CFRP laminates in the experimental study failed after yielding of reinforcement steel near the points of load application. As such, increasing μ will increase the flexural capacity of the tension side in the sagging regions, allowing for higher MR to be obtained. However, increasing the beam thickness had a negative impact on the resulting MR percentages as depicted in Beams B10, B15 and B16. Regarding the effect of laminate thickness, MR was enhanced by 32% when the thickness was increased from 1.2 to 1.8 mm, but this enhancement was not less significant when laminate thickness further increased to 2.6 mm, achieving an MR enhancement of 27% compared to B10. This is because of the CFRP debonding that occurred in B18 as depicted in Figure 14, which infers that increasing the CFRP laminate thickness is not always in favor of MR enhancement.

Table 5. Results of specimens strengthened with NSM steel plates

Specimen	P_u	$M_{sag(FE)}$	$M_{hog(FE)}$	$M_{sag.el}$	$M_{hog.el}$	[%] of change, M_{sag}	[%] of change, M_{hog}	Average [%] of MR	% of MR enhancement
	kN	kN.m							
B1’	602	60.93	-179.07	94.04	-112.85	-35.21	58.68	47	
B2	718	71.18	-216.82	112.24	-134.69	-36.59	60.98	49	4
B3	776	73.24	-241.77	121.32	-145.59	-39.64	66.06	53	13
B4	663	72.40	-186.80	103.63	-124.35	-30.13	50.22	40	-14
B5	650	78.31	-168.38	101.57	-121.88	-22.89	38.16	31	-35
B6	768	88.87	-206.33	120.02	-144.03	-25.96	43.26	35	-26
B7	856	109.33	-209.27	133.73	-160.47	-18.24	30.41	24	-48
B8	611	59.58	-186.43	95.49	-114.59	-37.61	62.69	50	7
B9	656	62.81	-202.39	102.50	-123.00	-38.72	64.54	52	10

Table 6. Results of specimens strengthened with NSM CFRP laminates

Specimen	P_u	$M_{sag(FE)}$	$M_{hog(FE)}$	$M_{sag.el}$	$M_{hog.el}$	[%] of change, M_{sag}	[%] of change, M_{hog}	Average [%] of MR	% of MR enhancement
	kN	kN.m							
B10	491	63.72	-118.08	76.73	-92.07	-16.95	28.25	23	
B11	535	66.98	-133.47	83.57	-100.28	-19.86	33.09	26	17
B12	553	68.76	-138.90	86.38	-103.66	-20.40	34.00	27	20
B13	521	67.30	-125.90	81.41	-97.69	-17.33	28.88	23	2
B14	594	73.59	-149.61	92.75	-111.30	-20.66	34.43	28	22
B15	631	84.43	-146.58	98.57	-118.28	-14.35	23.92	19	-15
B16	794	108.40	-180.20	124.06	-148.88	-12.62	21.04	17	-26
B17	513	62.18	-132.22	80.18	-96.22	-22.45	37.42	30	32
B18	508	63.44	-127.36	79.45	-95.34	-20.15	33.59	27	19

3) Specimens with NSM GFRP Laminates

As shown in Table 7, the increase in f_{cu} improved the percentages of MR achieved as observed from the results of B19, B20 and B21. Regarding the effect of the steel reinforcement ratio, the increase from 0.47% to 0.67% had a negligible effect on enhancing MR as shown from the results of beams B19 and B22. However, a further increase of μ to 1.2% in B23 has significantly enhanced MR compared to B19. Similar to the beams strengthened with steel plates and the ones retrofitted with CFRP laminates, increasing the beam depth resulted in the reduction of the average percentage of MR as shown in the results of beams B19, B24 and B25. Moreover, increasing the laminate thickness to 1.8 mm in B26 and to 2.6 mm in B27 resulted in about 6% and 12% enhancement of MR, compared to B19 where the laminate thickness was 1.2 mm.

Table 7. Results of specimens strengthened with NSM GFRP laminates

Specimen	P_u	$M_{sag(FE)}$	$M_{hog(FE)}$	$M_{sag.el}$	$M_{hog.el}$	[%] of change, M_{sag}	[%] of change, M_{hog}	Average [%] of MR	% of MR enhancement
	kN	kN.m							
B19	475	65.33	-106.87	74.23	-89.07	-11.99	19.98	16	
B20	506	67.83	-117.58	79.13	-94.96	-14.29	23.82	19	19
B21	531	67.73	-130.27	83.04	-99.65	-18.44	30.73	25	54
B22	479	65.27	-108.73	74.77	-89.73	-12.71	21.18	17	6
B23	540	71.46	-127.14	84.39	-101.27	-15.33	25.54	20	28
B24	582	82.68	-125.52	90.90	-109.08	-9.04	15.07	12	-25
B25	721	104.09	-152.11	112.59	-135.11	-7.55	12.58	10	-37
B26	483	65.95	-109.86	75.55	-90.65	-12.71	21.18	17	6
B27	486	65.77	-111.53	75.96	-91.15	-13.41	22.36	18	12

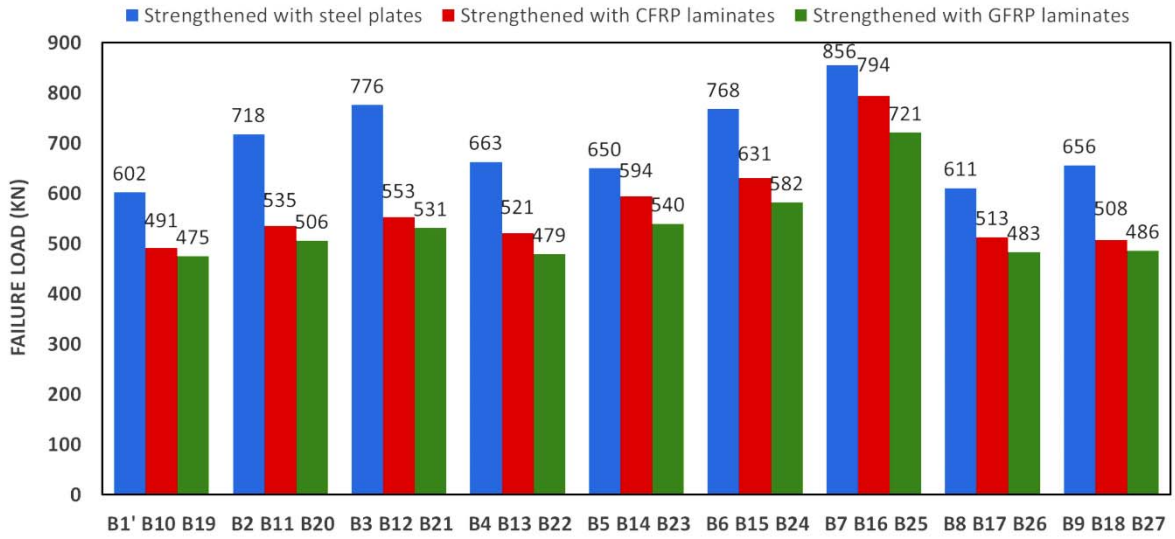

Figure (16): Failure loads for NSM-strengthened beams

4) Comparison of Results

Generally, all beams strengthened with steel plates have achieved higher MR than those strengthened using either CFRP or GFRP laminates. For example, the MR achieved in B1' increased by 104% and 194% compared to B10 and B19, respectively. Moreover, the difference in MR percentages increased as concrete compressive strength increased, whereas it was reduced with the increase in μ. Regarding the effect of the beam depth, the difference in MR ratios was the highest at 350 mm beam thickness, whereas that difference was reduced when the beam depth was increased to 450 mm. The difference in MR ratios was further reduced for beams with a beam depth of 550 mm, because increasing the

beam thickness enhances the strength of the beam, which allows for more moments to be redistributed toward the negative moment zone, resulting in compression failure due to concrete crushing. The highest recorded value for MR was 53% in steel-plated beams, compared to 30% and 25% using CFRP and GFRP strengthening, respectively, affirming the finding from the experimental program that NSM steel strengthening was more effective than NSM CFRP strengthening in terms of percentages of MR achieved. Steel strengthening also resulted in higher ultimate loads than the application of either CFRP or GFRP retrofitting for all the analyzed beams, as shown in Figure 16.

CONCLUSIONS

A novel strengthening technique is proposed for continuous reinforced concrete beams with accessibility restrictions from the bottom side. Strengthening was achieved by installing steel plates or CFRP laminates using a near-surface mounted technique at the hogging zone only. The proposed technique was assessed experimentally by testing five beams and was assessed numerically using validated finite element models. The numerical models were further used to perform a parametric investigation to assess the parameters that influence the efficiency of the proposed strengthening technique. A number of conclusions were reached and are listed as follows:

- Moment redistribution took place in the tested continuous beams before the plastic moment value was reached. The elastic moment redistribution occurred due to the variation in the flexural rigidity of the section throughout the span as a result of the plate installation and because of concrete cracking at critical sections.
- When applying top NSM CFRP laminates, the flexural stiffness of the specimens was not considerably affected.
- The application of top NSM steel plates, CFRP and GFRP laminates caused up to 50%, 30% and 25% MR, respectively, toward the negative moment zones.
- The application of two strengthening NSM steel plates would further enhance the MR behavior if more precautions were taken to avoid compressive failure due to concrete crushing.
- Redistribution of bending moments from sagging to hogging zones commences after the formation of cracks at the negative moment zones rather than after yielding of reinforcement.
- The resulting MR increases by increasing the concrete compressive strength regardless of the material of the strengthening plates.
- MR is enhanced by increasing the thickness of the strengthening steel plates or FRP laminates. However, debonding of the NSM CFRP laminates occurs in the case of using a laminate thickness higher than 1.8 mm at upper flexural stresses above 300 MPa.

REFERENCES

ABAQUS. (2014). “Theory manual, version 6.14”. Dassault Systems.

Akiel, M.S., El-Maaddawy, T., and El Refai, A. (2018). “Serviceability and moment redistribution of continuous concrete members reinforced with hybrid steel-BFRP bars”. Construction and Building Materials, 175, 672-681.

American Society for Testing and Materials. (ASTM). (2000). “Designation E8M-04: Standard test methods for tension testing of metallic materials [metric]”. Annual Book of ASTM Standards, ASTM International.

Ashour, A.F., El-Refaie, S.A., and Garrity, S.W. (2004) “Flexural strengthening of RC continuous beams using CFRP laminates”. Cement and Concrete Composites, 26, 765-775.

Aykac, S., Kalkan, I., Aykac, B., Karahan, S., and Kayar, S. (2013). “Strengthening and repair of reinforced concrete beams using external steel plates”. Journal of Structural Engineering, 139 (6), 929-939.

BS EN12390-3. (2009). “Testing hardened concrete- Part 3: Compressive strength of test specimens”. British Standards.

Carmo, R.N.F., and Lopes, S.M.R. (2008). “Available plastic rotation in continuous high-strength concrete beams”. Canadian Journal of Civil Engineering, 35 (10), 1152-1162.

De Lorenzis, L., Nanni, A., and Modena, C. (2002). "Bond between near-surface mounted fiber-reinforced polymer rods and concrete in structural strengthening". ACI Structural Journal, 99 (2), 123-132.

El-Refaie, S.A., Ashour, A.F., and Garrity, S.W. (2003). "Sagging and hogging strengthening of continuous reinforced concrete beams using carbon fiber-reinforced polymer sheets". ACI Structural Journal, 100 (4), 446-453.

Farahbod, F., and Mostofinejad, D. (2011). "Experimental study of moment redistribution in RC frames strengthened with CFRP sheets". Composite Structures, 93 (3), 1168-1177.

Fouda, M.A., El-Kateb, M., Elkateb, T., and Khalil, A. (2021). Numerical investigation for failure load and contact stress beneath RC square footing resting on cohesionless soil". Case Studies in Construction Materials, 15, e00656.

Fouda, M.A., Ibrahim, A., El-Kateb, M., Elkateb, T., and Khalil, A. (2022). "Numerical investigation for strengthened RC footings with square concrete jacketing". Case Studies in Construction Materials,16, e00807.

Hassan, T., and Rizkalla, S. (2003) "Investigation of bond in concrete structures strengthened with near-surface mounted carbon fiber-reinforced polymer strips". Journal of Composites for Construction, 7 (3), 248-257.

Ibrahim, A., Khalil, A., Salem, S., and El-Kateb, M. (2020). "Moment redistribution in continuous RC beams top-strengthened with steel and CFRP plates". International Journal of Recent Technology and Engineering, 8 (6), 3472-3480.

Ibrahim, A., Salem, S., Khalil, A., and El-Kateb, M. (2020). "Experimental investigation for moment redistribution in continuous RC beams top-strengthened with CFRP and steel plates". IOP Conference Series: Materials Science and Engineering, 809, 012007.

Ismail, S., Kaddah, F., and Raphael, W. (2020). Seismic soil structure interaction response of midrise concrete structures on silty sandy soil". Jordan Journal of Civil Engineering, 14 (1).

Jankowiak, T., and Lodygowski, T. (2005). "Identification of parameters of concrete damage plasticity constitutive model". Foundation of Civil and Environmental Engineering, No.6, Poznan University of Technology, Poland, 53-69.

Kara, I.F., and Ashour, A.F. (2013) "Moment redistribution in continuous FRP-reinforced concrete beams". Construction and Building Materials, 49, 939-948.

Lasheen, M., Shaat, A., and Khalil, A. (2018). "Numerical evaluation for the effective slab width of steel-concrete composite beams". Journal of Constructional Steel Research". 148, 124-137.

Li, L., Zheng, W., and Wang, Y. (2019). "Review of moment redistribution in statically indeterminate RC members". Engineering Structures, 196, 109306.

Liu, I., Oehlers, D.J., Seracino, R., and Ju, G. (2006). "Moment redistribution parametric study of CFRP, GFRP and steel surface plated RC beams and slabs". Construction and Building Materials, 20 (1-2), 59-70.

Liu, I.S.T., Oehlers, D.J., and Seracino, R. (2006). "Moment redistribution in FRP and steel-plate-reinforced concrete beams". Journal of Composites for Construction, 10 (2).

Lou, T., Lopes, S.M.R., and Lopes, A.V. (2014). "External CFRP tendon members: Secondary reactions and moment redistribution". Composites-Part B: Engineering, 57, 250-261.

Oehlers, D.J., Ju, G., Liu, I.S.T., and Seracino R. (2004a). "Moment redistribution in continuous plated RC flexural members. Part 1: Neutral axis depth approach and tests". Engineering Structures, 26, 2197-2207.

Oehlers, D.J., Ju, G., Liu, I.S.T., and Seracino, R. (2004b). "Moment redistribution in continuous plated RC flexural members. Part 2: Flexural rigidity approach". Engineering Structures, 26, 2209-2218.

Rahman, S.M.H., Mahmoud, K., and El-Salakawy, E. (2017). "Moment redistribution in glass fiber-reinforced polymer-reinforced concrete continuous beams subjected to unsymmetrical loading". Engineering Structures, 150, 562-572.

Rakgate, S. M., and Dundu, M. (2018). "Strength and ductility of simple supported R/C beams retrofitted with steel plates of different width-to-thickness ratios". Engineering Structures, 157, 192-202.

Scholz, H. (1993) "Contribution to redistribution of moments in continuous reinforced concrete beams". ACI Structural Journal, 90 (2), 150-155.

Wight, J.K., and James, M.G. (2012). "Reinforced concrete: Mechanics and design". Pearson.